Bi@hemistry

pubs.acs.org/biochemistry Article

An Allosteric Binding Site on Sortilin Regulates the Trafficking of VLDL, PCSK9, and LDLR in Hepatocytes

Robert P. Sparks, Andres S. Arango, Jermaine L. Jenkins, Wayne C. Guida, Emad Tajkhorshid, Charles E. Sparks, Janet D. Sparks, and Rutilio A. Fratti*



Cite This: *Biochemistry* 2020, 59, 4321–4335



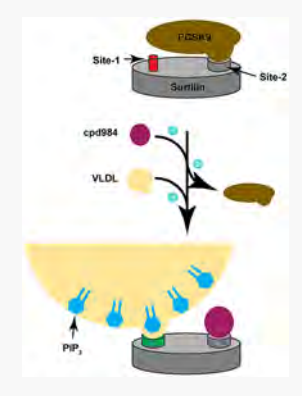
Read Online

ACCESS

Metrics & More

Article Recommendations

ABSTRACT: ApoB lipoproteins (apo B-Lp) are produced in hepatocytes, and their secretion requires the cargo receptor sortilin. We examined the secretion of apo B-Lp-containing very low-density lipoprotein (VLDL), an LDL progenitor. Sortilin also regulates the trafficking of the subtilase PCSK9, which when secreted binds the LDL receptor (LDLR), resulting in its endocytosis and destruction at the lysosome. We show that the site 2 binding compound (cpd984) has multiple effects in hepatocytes, including (1) enhanced Apo-Lp secretion, (2) increased cellular PCSK9 retention, and (3) augmented levels of LDLR at the plasma membrane. We postulate that cpd984 enhances apo B-Lp secretion in part through binding the lipid phosphatidylinositol 3,4,5-trisphosphate (PIP₃), which is present at higher levels on circulating VLDL form fed rats relative to after fasting. We attribute the enhanced VLDL secretion to its increased binding affinity for sortilin site 1 induced by cpd984 binding site 2. This hinders PCSK9 binding and secretion, which would subsequently prevent its binding to LDLR leading to its degradation. This suggests that site 2 is an allosteric regulator of site 1 binding. This effect is not limited to VLDL, as cpd984 augments binding of the neuropeptide neurotensin (NT) to sortilin site 1. Molecular dynamics simulations demonstrate that the C-terminus of NT (Ct-NT) stably binds site 1



through an electrostatic interaction. This was bolstered by the ability of Ct-NT to disrupt lower-affinity interactions between sortilin and the site 1 ligand PIP₃. Together, these data show that binding cargo at sortilin site 1 is allosterically regulated through site 2 binding, with important ramifications for cellular lipid homeostasis involving proteins such as PCSK9 and LDLR.

Human sortilin is an ancient protein transporter, which derived its origin from primitive eukaryotes. The gene for the sortilin orthologue in Saccharomyces cerevisiae is VPS10,1 which encodes a protein mainly responsible for trafficking vacuolar proteases to the vacuole. Yeast Vps10 is predicted to contain two separate and unique binding domains for protein sorting, increasing its molecular weight to ~173 kDa, whereas sortilin in humans is synthesized only as an ~93 kDa protein with one luminal β -propeller binding domain. The canonical Vps10 pathway in yeast transports the lysosomal protease carboxypeptidase Y (CPY) from the Golgi to the vacuole, after which Vps10 is taken back to the Golgi through a retrograde pathway defined by the retromer protein complex. The interaction of Vps10 with the retromer complex is facilitated through interactions with the cytoplasmic tail of Vps10 and the Rab Ypt7.3 The mammalian orthologue sortilin transports proteins from the Golgi, where it is activated by furin-mediated cleavage of its pro-domain, and is responsible for transporting its ligands between secretory pathways and lysosomal protein pathways. Both Vps10 and sortilin release cargo upon entering acidic endosomal compartments, which may be followed by dimerization of the luminal β -propeller domains. Subsequently, sortilin like Vps10 can be recycled back to the Golgi by the retromer pathway.

In higher eukaryotes, sortilin is expressed in diverse cell types where it serves as a tissue specific cargo receptor. In neuronal cells, sortilin mediates the secretion of neurotensin (NT) and other neuromodulators, while in adipose tissue, sortilin transports the type 4 glucose transporter Glut4 to the plasma membrane. That said, sortilin has recently been studied in hepatocytes where it primarily regulates apo B-containing lipoproteins (Apo-Lp) sorting through apo B binding; however, roles for apo E binding and PCSK9 regulation in hepatocytes have been examined. ^{8,10}

Through GWAS analysis, SORT1 mutations that correlate with cardiovascular disease outcomes have been identified. ^{11,12} Sortilin has complex relationships with lipoprotein metabolism ¹³ and with accumulation of lipids in arteries. ¹⁰ This is illustrated by the buildup of circulating LDL, the level of which can be increased when LDLR is endocytosed and degraded by binding PCSK9. At the plasma membrane, sortilin is found in

Received: September 4, 2020 Revised: October 28, 2020 Published: November 5, 2020





clathrin-coated pits similar to the low-density lipoprotein (LDL) receptor (LDLR), both of which bind apo B-Lp. ¹⁴ Differences in the function and ligand specificity of the two receptors are unknown. Further complicating our understanding of sortilin function is its additional role in hepatic very low-density lipoprotein (VLDL) secretion, where hepatic knockouts of sortilin have been described to increase or decrease VLDL secretion ¹⁵

Sortilin is a multiligand receptor that can interact with the various ligands found on VLDL, including B100,13 apo E,16,17 and phosphatidylinositol 3,4,5-trisphosphate (PIP₃). 18 The PIP₃ content of circulating VLDL is enriched relative to those of highdensity lipoprotein (HDL) and low-density lipoprotein (LDL). The paradox of the ability of sortilin to increase or decrease VLDL secretion under different conditions could relate to the relative concentration and position of ligands on the VLDL surface. The presence of PIP₃ on lipoproteins is related to insulin signaling, where PIP3 is considered as a principal mediator of insulin signal transduction. The presence of PIP₃ on VLDL could reveal a mechanism for short-term modulation of interaction of VLDL with sortilin, though we cannot at present rule out a role for other apo B-Lp ligands for binding of sortilin to VLDL such as apo E. 19,20 Overall, our results favor the concept that VLDL composition determines secretion and postsecretion pathways for VLDL catabolism.

An additional ligand transported by sortilin is PCSK9 (proprotein convertase subtilisin-kexin type 9), which has been shown to bind to human sortilin with high affinity. Importantly, another study showed that NT, a natural neuronal ligand for sortilin, did not inhibit PCSK9 binding, even at saturating concentrations, 22 suggesting the presence of an additional binding site on sortilin. Once PCSK9 is released by sortilin extracellularly, it binds to LDLR, triggering its internalization and degradation of the associated complex at the lysosome. This results in a decreased level of expression of LDLR on the cell surface, which can lead to eventual increases in the level of circulating LDL.

In this study, we present data showing that binding sortilin site 2 with compounds such as cpd984 increases PCSK9 cellular retention while increasing VLDL secretion. Conversely, the binding of sortilin site 1 with cpd541 decreases VLDL secretion. We suggest that this pathway is a complex and dynamic system for regulating the metabolism of apo B-containing lipoproteins, including LDL and its precursor VLDL, utilizing both binding sites on sortilin for regulation. We propose that site 2 allosterically regulates binding to site 1 to affect the coregulation of apo B and PCSK9 secretion, with the balances of this mode of modulation translating to changes in LDLR expression at the plasma membrane.

■ METHODS AND EXPERIMENTAL DETAILS

Cell Culture, Materials, and Reagents. McArdle (McA) RH-7777 cells were cultured as previously described in serum containing complete Dulbecco's modified Eagle's medium (cDMEM). Human sortilin (sortilin) (S78-N755) with a C-terminal six-His tag was from R&D Systems. Rabbit polyclonal PCSK9 (Ab125251, 1:2000) and LDLR (LS.C146979, 1:2000) antibodies were from LSBio. Mouse anti-glyceraldehyde phosphate dehydrogenase (GAPDH) from Santa Cruz Biotechnology [sc32233 (6C5), 1:200]. Lipofectamine 2000, Plus Reagent was from Thermo Fisher. Anti-rabbit (NA934, 1:10000) and anti-mouse (NA931, 1:10000) horseradish peroxidase (HRP)-linked IgG and Hyperfilm were

purchased from GE Healthcare. Horseradish peroxidase-linked donkey anti-rabbit IgG (NA9340, 1:10000), sheep anti-mouse IgG (NXA931, 1:10000), and ECL Prime Western Blotting Detection Reagent (RPN2232) were from GE Healthcare. Compound 98477898 $\{(2S)-1-\text{methyl } N-3-[(3-1)]\}$ phenypropanoyl)amino]phenylpyrrolidine-2-carboxamide (cpd984) and compound 54122218 ({[(2-{[(1R)-1phenylethyl amino carbonyl) phenyl amino acetic acid) were obtained from ChemBridge Corp. Stock solutions of cpd984 and cpd541 (10 mM) were prepared in DMSO and stored in aliquots at -20 °C. DPPC (dipalmitoyl-sn-glycero-3-phosphatidylcholine) and POPE (1-palmitoyl-2-oleoyl-sn-glycero-3phosphatidylethanolamine) were purchased from Avanti Polar Lipids (Alabaster, AL) as chloroform stock solutions and stored at 20 °C. DiC16 PIP₃ (dipalmitoylphosphatidylinositol 3,4,5trisphosphate) and diC8 PIP₃ (dioctanoyl PIP₃) were from Echelon (Salt Lake City, UT). CM7 and Ni-NTA (standard and S series) sensor chips and regeneration buffers (glycine pH 1-3) were procured from GE Healthcare (Buckinghamshire, U.K.). Monolith NT.115 standard treated capillaries for thermophoresis were purchased from Nanotemper (München, Germany). Membrane scaffold protein 1SD1 (MSP) was prepared as described previously.2

Cell Culture. Rat hepatocytes (RH) were isolated from Sprague-Dawley rat livers and cultured on collagen-coated dishes in Waymouth's 751/1 medium containing 0.2% (w/v) BSA as described previously. Wild-type McA cells were maintained in culture in cDMEM. Inhibitors were used at reported concentrations for cpd984 and cpd541. Inhibitors were validated in RH where cell toxicity was minimal as determined by LDH release.

Knockdown of Sortilin in McA Cells Using siRNA. McA cells were transfected using Fugene6 according to the manufacturer's protocol (Promega Corp.) using three different pGIPZ-based vectors expressing shRNAi targeting rat Sort1 mRNA (V2LMM_58553, V3LMM_450660, and V3LMM_450662) and one scrambled, nonsilencing control (GE Healthcare Dharmacon) as previously described.²⁷ Puromycin selection was performed on McA cells. Sortilin knockdown from each cell line was examined by immunoblotting.

Immunoblotting. McA cell lysates were prepared, and denatured proteins were separated by sodium dodecyl sulfate—polyacrylamide gel electrophoresis, transferred to PVDF, and incubated with primary antibodies overnight at 4 °C in blocking buffer with antibody binding detected with species specific secondary HRP-linked antibodies and developed using Amersham Prime reagent (GE Healthcare). Chemiluminescence was measured with a ChemiDocXRS+ system (Bio-Rad) and quantified using Image Lab 3.0.1 software from Bio-Rad.

Lipoprotein Preparation and PIP₃ Nanodisc Assembly. Plasma VLDL, LDL, and high-density lipoprotein (HDL) from fasted rats were isolated by sequential density ultracentrifugation as previously described. Nanodiscs were prepared as described previously. Nanodiscs were composed of 3.023 μ mol of DPPC, 0.098 μ mol of diC16 PIP₃, and 0.78 μ mol of POPE, which were combined, dried, and desiccated overnight. Lipids were dissolved in 20 mM sodium deoxycholate in TBS [50 mM Tris-HCl (pH 7.4), 150 mM NaCl, and 0.02% (w/v) sodium azide] and sonicated, after which membrane scaffold protein 1D1 (MSP1D1) was added at a 70:1 lipid:protein ratio, and the detergent was removed with Bio-Beads SM-2 (Bio-Rad). Nanodiscs were isolated using size exclusion chromatography. The concentration of Nanodiscs was quantified using a

NanoDrop and an extinction coefficient of 21000 L mol⁻¹ cm⁻¹ for MSP1D1, and the resultant in milligrams per milliliter divided by 2.

Computational Modeling and Compound Screening. Schrödinger's Maestro program (version 9.3.5) was used as the primary graphical user interface, and Maestro version 10.2 (Schrödinger, LLC) was used for ligand interaction diagramming. Virtual screening was performed on compounds contained in ChemBridge libraries (www.chembridge.com) that were prepared with Schrödinger's LigPrep program (Schrödinger, LLC). The virtual screening method was performed using Schrödinger's GLIDE software²⁹ on the sortilin crystal structure of Protein Data Bank (PDB) entry 4PO7.²⁷ Compounds were docked on grids generated with Glide with cpd541 docked at a box determined by C-terminal NT and cpd984 docked at a box determined by the N-terminal fragment of NT. Grids were then adapted from alignment of PDB entries 6EHO and 4PO7 and docking performed for all grids using the Glide XP setting with results exported into GraphPad Prism.

MD Simulations of Apo and Holo Sortilin. Using the aforementioned crystal structure of sortilin (PDB entry 4PO7), molecular dynamics simulations were performed using NAMD 2.12³⁰ using the CHARMM36m force field.³¹ Prior to simulation, the system was prepared using the CHARMMGUI solution builder, with a salt concentration of 150 mM NaCl. Simulation parameters included a constant pressure of 1 atm via Langevin dynamics, as well as a constant temperature of 310 K using Langevin piston Nosé-Hoover methods. 32,33 Long-range electrostatic forces were evaluated using the particle mesh Ewald (PME) method with a 1 Å grid spacing. 34,35 van der Waals interactions were calculated using a 12 Å cutoff with a forcebased switching scheme after 10 Å, as well as a 2 fs time step integration via the SETTLE algorithm.36 Visualization and analysis were performed using VMD 1.9.3.³⁷ The system was equilibrated for 20 ns, restraining the $C\alpha$ atoms of the protein $(1.0 \text{ kcal mol}^{-1} \text{ Å}^{-2})$ to allow for solvation. This was followed by a production run of 50 ns without restraints for four poses taken from ensemble docking, three poses with the highest-affinity pose for site 1 of sortilin run in duplicate for each, and the pose for site 2 that represented the predicted pose as shown previously.²⁷ Compounds were docked using GLIDE at the site where the N-terminal fragment of NT is found in the crystal structure, and cpd984 was chosen for biological screening based on its docking score. Schrödinger's PRIME software was used to generate missing side chains and loops of this crystal structure, predicting the NT peptide spanning the cavity of sortilin as in ref 27. MD simulations were performed on full length NT as well as the three potential peptides derived from this structure using Schrödinger Maestro to manipulate the N-terminal density from this structure, converting it from a carboxylate to an amide. Schrödinger protein preparation wizard was run on the Cterminal density as well as the two N-terminal densities, and all three potential structures were minimized. The 50 ns simulations described above were performed on all three NT fragments, and root-mean-square deviations (RMSDs) of all three simulations and final poses from each simulation exported.

Ensemble Molecular Docking of cpd541 and cpd984. To probe interactions of cpd541 and cpd984 with sortilin, ensemble molecular docking was employed as described previously.³⁸ Using snapshots from the 50 ns production simulation to sample protein dynamics, snapshots were taken every 200 ps. Each of the resultant 250 snapshots was used to dock cpd541 and cpd984 using a 100 Å × 90 Å × 70 Å grid box.

Docking was performed with an exhaustiveness of 10, yielding a total of 2500 docked poses. Resultant poses were clustered using a hybrid K-centers/K-medoids algorithm, utilizing an RMSD method. Representative poses with the highest scoring affinities in clusters closest to sites 1 and 2 were selected for further 50 ns simulations. The resultant drug-bound simulations were analyzed with VMD as well as MDAnalysis. 41,42

Microscale Thermophoresis (MST). Thermophoresis measurements were performed using a Monolith NT.115 labeled thermophoresis instrument. 43 Sortilin-His6 was labeled with Ni-NTA Atto-488 according to the manufacturer's protocol as previously described. 44,45 M.O. Control software was used for MST. Target protein concentrations were 50 nM for sortilin-labeled protein. The light-emitting diode excitation power was set to 90%, and MST set to high allowing 3 s prior to MST on to check for initial fluorescence differences, 25 s for thermophoresis, and 3 s for regeneration after MST off. Analysis was performed using M.O. Affinity Analysis Software as the difference between the initial fluorescence measure in the first 5 s as compared with thermophoresis at $15\ s.$ All measurements were performed in PBS buffer [137 mM NaCl, 2.7 mM KCl, 8 mM Na₂HPO₄, and 2 mM KH₂PO₄ (pH 7.4)] without Tween, and the binding affinity was generated using Graphpad Sigmoidal 4PL fit from points exported from M.O. Affinity Analysis software using K_D Model with the target concentration fixed at 50 nM.

Surface Plasmon Resonance. SPR measurements were performed on a Biacore T200 instrument equipped with CM5 sensor chips with ~2000 response units (RU) of sortilin covalently immobilized to the surface for VLDL and LDL binding (6C and 6E), ~3500 RU cross-linked sortilin for small molecule binding (6A), a CM5 with ~6500 RU cross-linked sortilin for NT binding (5A), and a CM7 chip as in ref 18 (7A) and 7C). HBS-DMSO running buffer [10 mM HEPES (pH 7.4), 150 mM NaCl, and 1% DMSO was used at a flow rate of 30 μ L/min, and injections were performed with times for association of 90 s and dissociation of 300 s, followed by injection of buffer to regenerate the sortilin surface. Regeneration for CM5 NHS/EDC cross-linked sortilin required a 30 s injection of 10 mM NaOH as described previously. 18 Binding was expressed in RU, the difference in the response between the immobilized protein flow cell and the corresponding control flow cell. Results were exported from BiaEvaluate software into GraphPad Prism (GraphPad Software). cpd984 and cpd541 saturation curves were fit using a specific binding equation with a Hill slope, whereas all other SPR saturation curves were fit using a 1:1 specific binding model.

Statistics. Unless noted, results are expressed as the mean \pm the standard error of the mean (SEM), where n equals the number of independent experiments in which replicate analyses were performed in each experiment. Significant differences were assessed using one-way analysis of variance (ANOVA) with p values of \leq 0.05 being considered significant.

RESULTS

cpd984 and **cpd541** Bind at Different Locations of Human Sortilin. In a previous study, we defined the interaction of a small molecule compound (cpd984) with a newly defined second binding site (site 2) on the luminal β-propeller domain of sortilin, and its effects on the secretion of NT and VLDL. Here we define a small molecule (cpd541) that specifically targets site 1 on the opposite side of the β-propeller relative to site 2 (cpd984). Figure 1A shows the structures of both cpd984

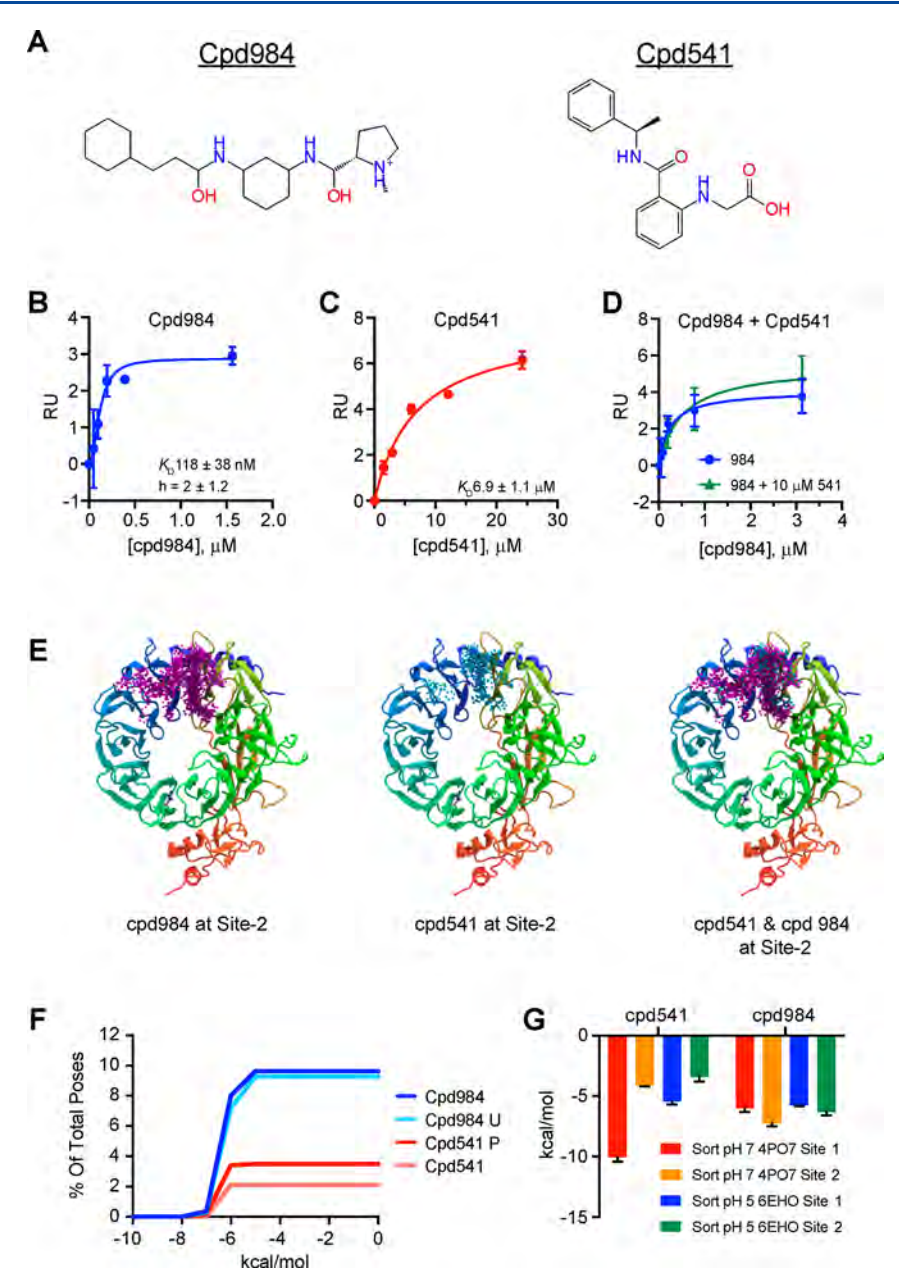


Figure 1. Experimental and computational characterization of cpd541 and cpd984. (A) Structures of cpd984 and cpd541. (B) SPR-determined binding affinity of cpd984 for a CM5 chip loaded with ~3000 RU of human sortilin with the saturation curve (blue) indicating a $K_{\rm D}$ of 118 \pm 38 nM. (C) SPR of cpd541 binding to sortilin with a saturation curve (red) $K_{\rm D}$ of 6.9 \pm 1.1 μ M. (D) SPR of binding a cpd984 titration in the presence (green) and absence (blue) of 10 μ M cpd541 with saturation curves. (E) Resultant poses from ensemble docking for cpd984 (purple) and cpd541 (cyan) at site 2 of sortilin alone and superimposed. (F) Percent of overall poses from ensemble docking vs relative docking score for cpd984 (red) and cpd541 (blue), where the Y axis is the percent of all poses for ensemble docking that bind site 2 of sortilin, with cpd984 having ~9% percent of all poses in site 2 and cpd541 having ~3% of all poses. (G) Schrödinger Glide Xp scores of cpd541 and cpd984 docked in sites 1 and 2 of pH ~7 PDB entry 4PO7 and pH ~5.5 PDB entry 6EHO.

and cpd541. Using SPR, we titrated cpd984 and showed that it bound to sortilin with a high affinity, having a $K_{\rm D}$ of 118 \pm 38 nM using GraphPad Prism versoin 8.4.3 using a specific binding with Hill slope model (Figure 1B). Next, we determined the binding affinity of sortilin for cpd541 and found the $K_{\rm D}$ to be 6.9 \pm 1.1 μ M using the same model (Figure 1C). To determine whether binding of site 2 was independent of that of site 1, we measured the binding of cpd984 in the presence of a nearly saturating concentration of cpd541 (10 μ M), showing that cpd984 bound to sortilin with a similar affinity in the presence and absence of cpd541 just looking at the saturation curves visually (Figure

1D). This indicated site specificity of cpd984 for site 2 of sortilin and that its binding was independent of site 1 interactions when coupled to previous results utilizing this compound.²⁷ These results are consistent with our previous study showing that cpd984 bound sortilin in the presence of the C-terminal portion of NT.¹⁸

We employed state-of-the-art computational techniques to further explore the site specificity of these molecules with respect to sortilin. Using ensemble molecular docking, we showed the association of cpd984 and cpd541 with regions of sortilin site 2. This showed that cpd984 associated with site 2

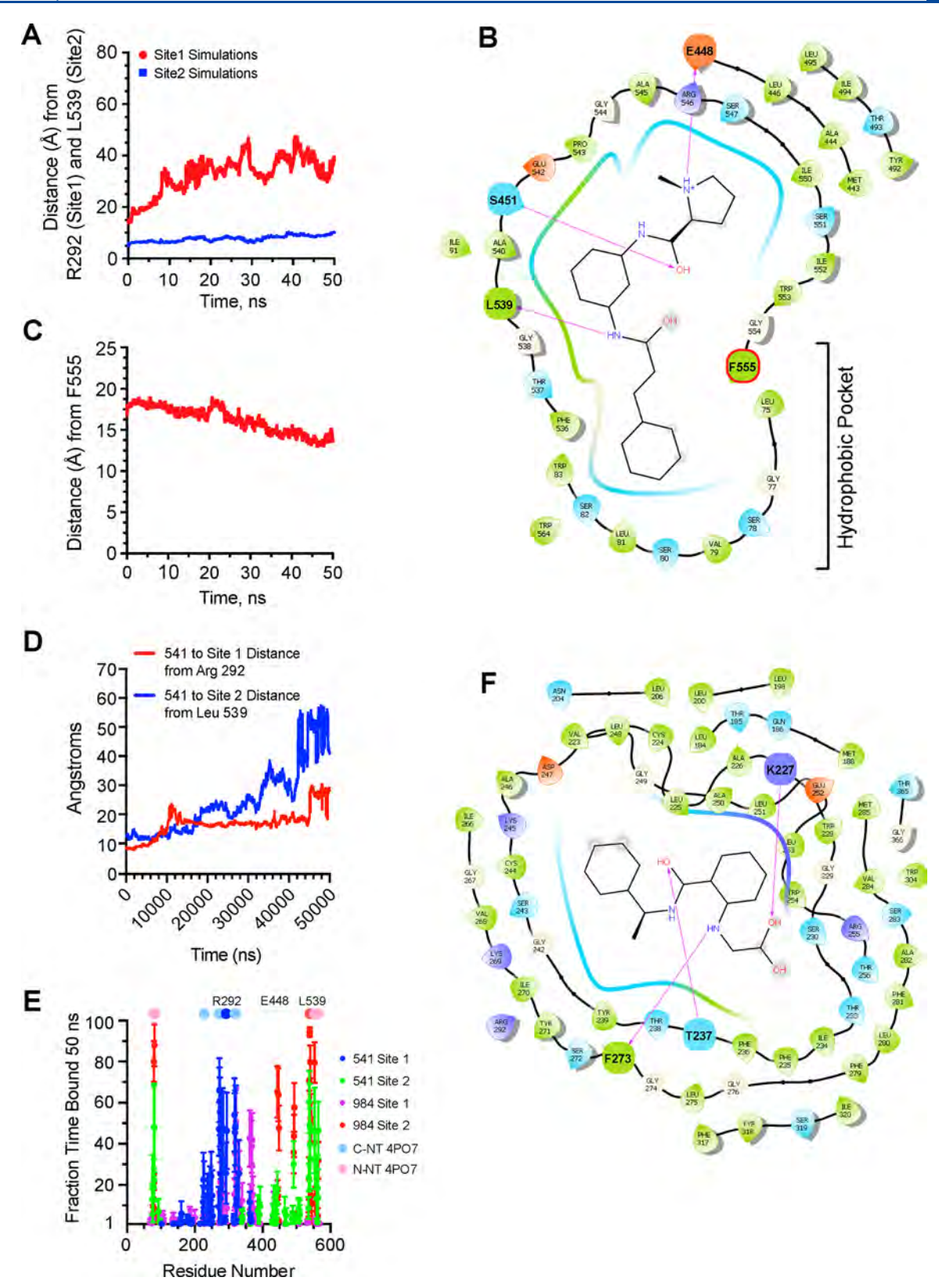


Figure 2. Molecular dynamics simulations of cpd984 with respect to sortilin site 1 and 2. (A) Simulations of bound cpd984 poses taken from ensemble docking as in panels D and E of Figure 1 with the site 2 pose taken from the closest ensemble docking from pose to pose (n = 6) and the three highest-scoring poses for cpd984 with respect to site 1 (n = 2 each) based on ensemble docking. Center of mass differences over time (50 ns) between cpd984 and a representative residue of site 1 (R292) for the three duplicate simulations of cpd984 with respect to site 1 are colored red, whereas center of mass differences between cpd984 and a representative residue of site 2 (L539) for the six duplicate simulations of cpd984 with respect to site 2 are colored blue. (B) Ligand interaction diagram taken from a representative simulation from panel A of cpd984 with respect to site 2 of sortilin at the end of the 50 ns MD simulation. (C) Center of mass difference over time as in panel A between cpd984 and a representative residue of the hydrophobic ligand binding pocket of sortilin adjacent to site 2 (F555) of six simulations of site 2-bound ligands. (D) Simulations of bound cpd541 as in panel A, with the

Figure 2. continued

center of mass taken from R202 and L539 as in panel A, from top three cpd541 ensemble docking poses in site 2 (n = 2) and cpd541 poses from site 1 with a salt bridge between cpd541 and R292. (E) Residue analysis for all 24 of the 50 ns simulations of cpd984 and cpd541 in sites 1 and 2 of sortilin with the fraction time bound calculated by determining number of frames (5000) in which a residue of sortilin was within 3.5 Å of either cpd984 or cpd541. C-term and N-term NT used as a legend at 100% over the one frame taken from PDB coordinates of PDB entry 4PO7. (F) Ligand interaction diagram taken from a representative simulation from panel D of cpd541 with respect to site 1 of sortilin at the end of the 50 ns MD simulation.

with a rate of contact that was higher than that of cpd541 (Figure 1E). When quantitated, cpd984 was associated with contact site 2 with a rate that was 2-fold greater than that of cpd541 (Figure 1F). Furthermore, we found that cpd984 with an unprotonated pentaamine ring had a basic pH of 8.4 \pm 1.2, as determined by ab initio calculations using Jaguar. 46 The protonation state of cpd984 had no effect on site 2 binding, whereas cpd541 protonation of the carboxylate resulted in the enrichment of cpd541 at site 2 of sortilin. To test whether pH-dependent conformational changes impacted site 1 or site 2 binding, using Schrödinger Glide XP, we computationally docked both cpd541 and cpd984 in both sites 1 and 2 of a crystal structure of sortilin at neutral pH (PDB entry 4PO7) and acidic pH (PDB entry 6EHO) (Figure 1G). cpd541 showed dramatically weakened binding to sortilin site 1 at low pH as compared to cpd984, indicating that cpd541 is similar to other site 1 ligands that bind to the NT binding site of sortilin and lose affinity in acidic environments.6 Furthermore, docking results confirm that cpd984 shows little discrimination between acidic- and neutral-pH structures of sortilin.

Using MD, six 50 ns simulations were run for cpd541 and cpd984 to both sites 1 and 2 of sortilin totaling 24 simulations and >1 μ s of total simulation time (Figure 2A). The three best binding poses of cpd984 with respect to site 1 were chosen using ensemble poses generated from clusters of site 1, whereas the three best poses with a salt bridge from cpd541 to R292 with the best autodock docking score were chosen and all three poses run in duplicate for 50 ns each. For site 2, we used the cpd984 pose with the closest match to our previously determined pose for binding of cpd984 to sortilin site 2.27 In comparison, the three best poses of cpd541 with respect to site 2 nearest to previously reported L539 were used.²⁷ We found that cpd984 remained within 10 Å of L539 throughout the simulation (Figure 2A). In contrast, simulations of cpd984 with respect to site 1 showed that it did not stay within 10 Å of R292 for site 1. In addition to the stable association of cpd984 with site 2, we found that cpd984 buries itself in the hydrophobic sortilin β -propeller, between blades 1 and 10. Using F555 as a reference amino acid near the end of blade 10 of sortilin, we show that cpd984 on average over six 50 ns simulations comes closer to this hydrophobic cavity over time (Figure 2C). A representative end point of one of these simulations is presented with a ligand interaction diagram in Figure 2B. Altogether, we hypothesized that the hydrophobic cpd984 was more likely to stay bound to site 2 than to site 1. Additionally, as cpd984 does not carry a negative charge at acidic or neutral pH and has stronger association with site 2 than site 1 of sortilin, it was likely that binding of cpd984 to sortilin was independent of pH in the cell.

With regard to cpd541, we hypothesized that it required some electrostatic binding to form a salt bridge with R292 and stably interact with site 1 via its carboxylate. Our data show that cpd541 did not stay as tightly associated with site 2 of sortilin as compared to cpd984 (Figure 2D). In contrast, cpd541 stably associated with site 1. That said, not all cpd541 simulations remained associated with R292. A fraction of cpd541

simulations started with a salt bridge to R292, eventually stably forming a salt bridge with K227 depicted in one of the final frames of a cpd541 simulation with respect to site 1 of sortilin (Figure 2F).

To visualize the interactions of cpd984 and cpd541 with different residues on sortilin, we analyzed individual contacts over time in all MD simulations (n = 24) to determine whether either cpd541 or cpd984 stayed within 3.5 Å of a given residue of sortilin. Here, each of the 50000 frames analyzed represents 1 ps. From this, it was clear that cpd984 had a greater fraction bound in site 2 relative to that of cpd541 using this rubric, and that cpd541 had a greater fraction of time bound to site 1 (Figure 2E). Furthermore, the residues of interest for these interactions corresponded well to the NT peptide binding modes of sortilin from PDB entry 4PO7, which we have hypothesized represent the full NT peptide across the sortilin cavity connecting sites 1 and 2 of sortilin. 27

Modulation of PCSK9 and LDLR by cpd984. While the computational work described above was essential to determine how and where these compounds interact with sortilin, it was important to investigate the downstream effects on biological sortilin ligands. For this purpose, we used the McCardle hepatocyte (McA) cell line to examine sortilin-mediated trafficking of PCSK9 and LDLR when cells were treated with cpd984 and cpd541. We found that treatment with 10 μ M cpd984 increased the level of intracellular PCSK9, suggesting that its secretion was reduced by cpd984-sortilin interactions (Figure 3A). This also showed a significant increase in the total amount of LDLR of >2-fold. Because LDLR is membraneanchored and is known to be degraded through the endolysosomal pathway, the effect of cpd984 can be attributed to inhibition of degradation of PCSK9 by the lysosome. Importantly, the administration of 10 μ M cpd541 had little effect on the level of PCSK9 or LDLR. These results led us to hypothesize that increased cellular PCSK9 corresponded to its decreased secretion, which would serve as an explanation for subsequent reduction of the endocytosis and degradation of LDLR-PCSK9 complexes. On the basis of these observations, we posit that cpd984 administration results in increased sortilin-VLDL binding, reducing the availability of sortilin to bind to PCSK9.

A Sortilin-Targeting Small Molecule Alters NT Binding and Apo B Secretion. The effect of cpd984 on PCSK9 binding suggested that other sortilin cargo could be affected by allosteric conformational changes of sortilin. We first examined the dependence of sortilin levels on the effect of cpd984. This was done utilizing siRNA to differentially knock down sortilin expression in McA cells. Sortilin knockdown cell lines 1–4 expressed 95%, 70%, 40%, and 10% of sortilin, respectively, relative to the scrambled siRNA control cells (Figure 4A). Using these McA cell lines, we measured apo B secretion with 10 μ M cpd984 and found that cpd984 enhanced apo B secretion in proportion with sortilin expression. We hypothesized that binding site 2 with cpd984 allosterically enhanced the binding of VLDL at site 1, which would explain the increased secretion of

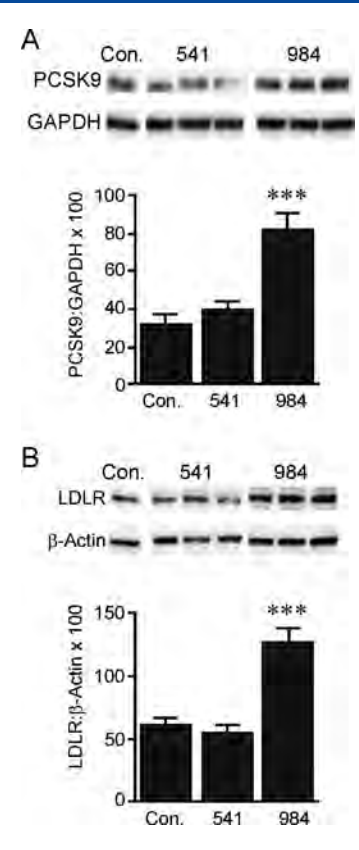


Figure 3. Biological effect of cpd984 and cpd541 treatment in McCardle cells on cellular PCSK9 and LDLR levels. McA cells were incubated in 1% BSA/DMEM with DMSO, cpd541 (10 μ M), or cpd984 (10 μ M) for 18 h. Cellular proteins were extracted and analyzed by immunoblotting for (A) LDLR (LS-C146979, 1:2000) or (B) PCSK9 (Ab125251, 1:2000) using the HRP-linked secondary antibody and ECL detection. Loading controls included β -actin (Rockland ph600-401-886, 1:1000) and GAPDH [sc-32233 (6CS), 1:200]. Band intensities were measured using the ChemiDocXRS+ system and evaluated using ImageLab 5.1 software. Error bars represent the SEM (n = 3). ***p < 0.001 (one-way ANOVA with multiple comparisons).

VLDL. This also shows that sortilin is the rate-limiting ligand and that overall cellular effects of site specific sortilin modulation represent trafficking balances within the cell. In parallel, we tested whether this trend held when cells containing normal levels of sortilin were incubated with increasing concentrations of the site 1 and site 2 specific molecules. To do this, we varied the concentrations of cpd984 and cpd541 with cells expressing wild-type levels of sortilin. These results showed that cpd984 enhanced apo B secretion in a dose-dependent manner (Figure 4B). cpd541, on the contrary, showed a dose-dependent inhibition of apo B secretion. This is in keeping with the notion that binding site 2 with cpd984 allosterically affected interactions of site 1 with apo B.

Characterization of VLDL and LDL Sortilin Affinity. Having concluded previously that PIP₃ binds to site 1 of sortilin, 17 we tested the effects of cpd541 and cpd984 on binding of PIP3 to sortilin to determine whether binding of PIP3 to sortilin could be allosterically modulated through site 2 on sortilin. SPR experiments showed that soluble short chain diC8 PIP₃ bound with high affinity to cross-linked sortilin with a K_D of $4.2 \pm 0.4 \,\mu\mathrm{M}$ using the GraphPad Prism version 8.4.3 specific binding with a Hill slope model (Figure 5A). When we tested the same diC8 PIP₃ concentration curves in the presence of 10 μ M cpd541 and 10 μ M cpd984, we found that cpd541 abolished PIP₃ binding, whereas cpd984 enhanced binding of diC8 PIP₃ to sortilin by 10-fold with a K_D of 474 \pm 85 nM using the same fit in Figure 5A. These data suggest that binding of PIP₃ to site 1 can be regulated by site 2 conformational changes and demonstrate that the effect of cpd984 is not limited to the apo B ligand present on the VLDL surface. To determine if these effects held true for more native forms of PIP3 that might be available for sortilin binding, we used nanodiscs containing 2.5% diC16 PIP₃. Sortilin-bound PIP3 nanodiscs with an increased binding affinity over diC8 PIP₃ for sortilin with a K_D of 55 \pm 13 nM indicated that a full bilayer is important for the interaction between PIP₃ and sortilin binding, where cpd984 augmented the affinity of this interaction by 10-fold for a K_D of 5.4 \pm 0.8 nM using the GraphPad Prism version 8.4.3 one-site specific binding model for both fits (Figure 5B).

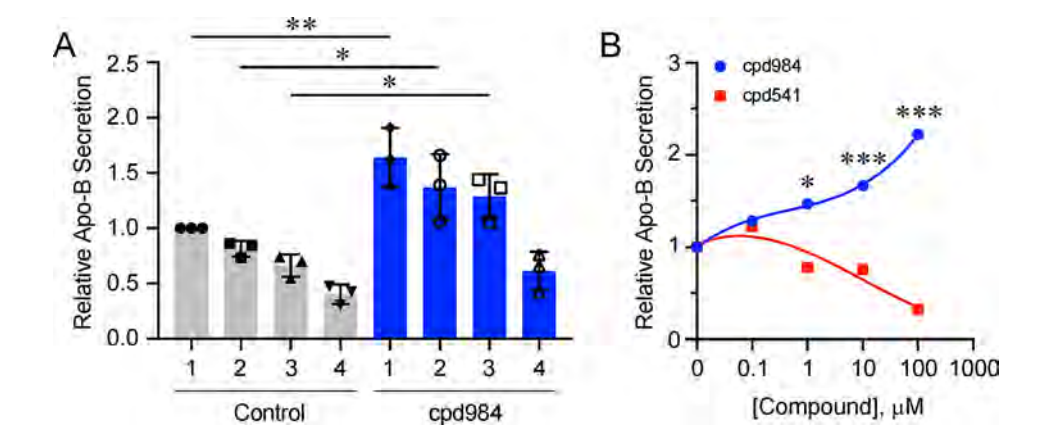


Figure 4. cpd984 increased LDLR levels and decreased PCSK9 levels. (A) McA cell knockdowns with varying levels of sortilin were measured for secretion of VLDL-B100 into medium and assessed by an immuno-slot blot. Sortilin knockdown cell lines 1-4 expressed 95%, 70%, 40%, and 10% of sortilin, respectively, relative to the scrambled siRNA control cells. Cells were treated with $10 \,\mu\text{M}$ cpd984 or medium alone (1% BSA/DMEM). Results are the average of triplicate plates for each condition. Error bars represent the SEM (n=3). *p<0.05, and **p<0.01 (one-way ANOVA with multiple comparisons). (B) Insulin sensitive McA cells were incubated with increasing concentrations of cpd541 or cpd984, and secretion of VLDL-B100 into medium was assessed by an immuno-slot blot. Each curve was normalized to $0 \,\mu\text{M}$ treatment that was set to 1. Error bars represent the SEM (n=3). *p<0.05, and ***p<0.001 (two-way ANOVA with multiple comparisons).

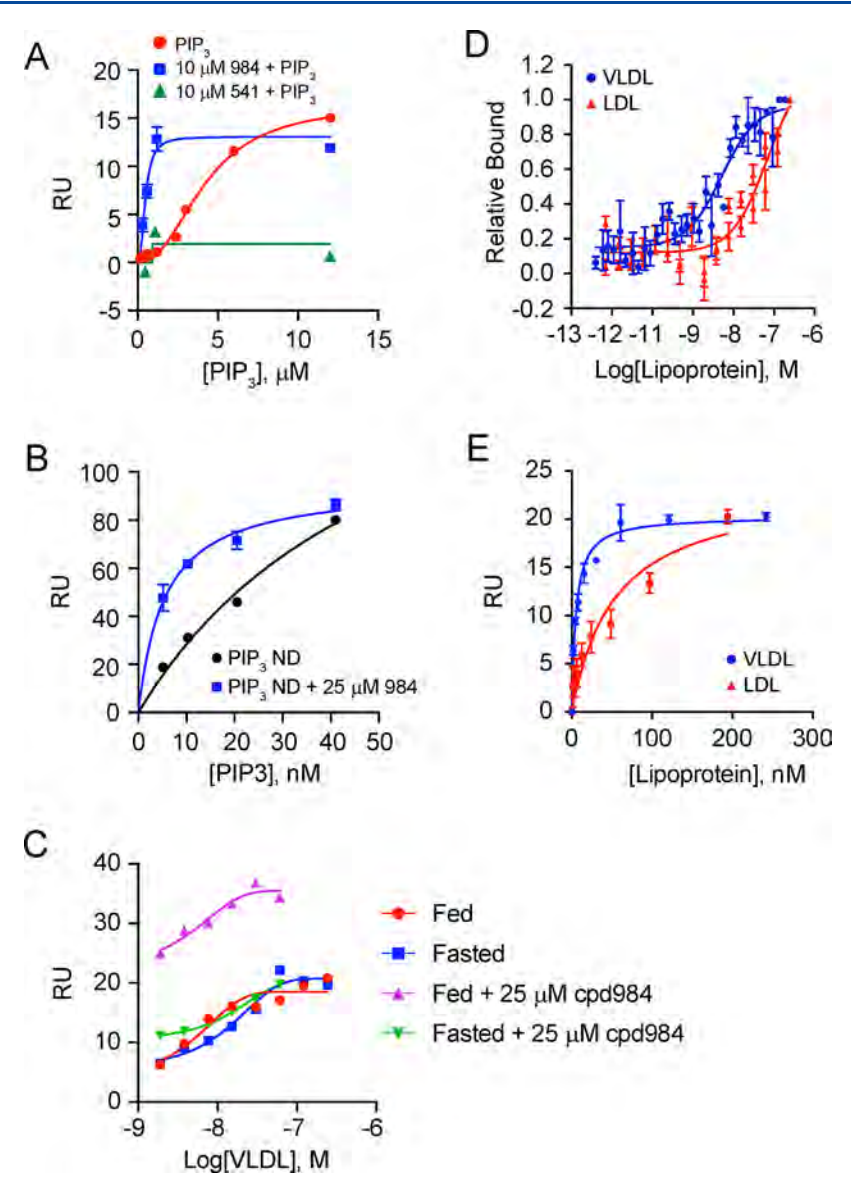


Figure 5. SPR of sortilin—lipoprotein binding. (A) SPR as in Figure 1A of diC8 PI(3,4,5)P₃ binding measurements in the presence and absence (red) of $10\,\mu\mathrm{M}$ cpd984 (blue) and cpd541 (green) indicating diC8 PIP₃ bound with a K_D of $4.2\pm0.4\,\mu\mathrm{M}$, which was enhanced to a K_D of 474 ± 85 nM in the presence of cpd984. (B) SPR analysis using PIP₃ nanodiscs was performed using a CM7 chip containing ~27000 RU of sortilin indicating a binding affinity K_D of 54 nM, which was enhanced roughly 10-fold in the presence of 25 $\mu\mathrm{M}$ cpd984. (C) SPR of binding of sortilin to VLDL fed fraction in the presence of cpd984. Otherwise, no difference was found in the saturation curves for binding of VLDL to sortilin harvested from rats being fed and fasted. (D) Labeled microscale thermophoresis (MST) using Atta-647 Ni-NTA-labeled sortilin (12.5 nM) measured with 32 different concentrations of VLDL and LDL run in triplicate and analyzed using Nanotemper M.O. Affinity Analysis software with K_D values for VLDL of ~4 nM and for LDL of ~74 nM. (E) SPR performed using a CM5 chip containing ~2000 RU of sortilin of circulating rat VLDL lipoprotein fed and fasted fractions pooled for overall K_D values for VLDL of ~5 nM and for LDL of ~54 nM.

In vivo, levels of PIP $_3$ are increased under conditions of insulin stimulation. We hypothesized that VLDL harvested under conditions of insulin stimulation would show increased binding to sortilin as compared to that of VLDL isolated under conditions of decreased insulin. To test this, we used VLDL purified from fed and fasted rats. VLDL samples were titrated [n = 2 on two different chips; CM7 data also used (not shown)] over sortilin attached to a CM5 chip with ~2000 RU of sortilin, and we found the $K_{\rm D}$ for fed VLDL using a 95% confidence interval and GraphPad Prism version 8.4.3 one-site specific binding model to be between 2.87 and 5.27 nM and between 3.96 and 10.8 nM for fasted VLDL (Figure 5C). In the presence of cpd984, the binding affinities were shifted higher for both fed and fasted rats with 95% confidence intervals of 404 pM to 1.47

nM for fed VLDL and 400 pM to 4.71 nM for fasted VLDL in the presence of 25 μ M cpd984. The difference in measured binding affinity between fed and fasted VLDL fractions in the presence of cpd984 showed double the amount of VLDL bound to sortilin harvested from fed rats (Figure 5C). These data lend support to the hypothesis that insulin signaling might affect VLDL particle composition, resulting in altered trafficking patterns that depend on the protein sorting chaperone sortilin. These data are consistent with the hypothesis that binding of sortilin to VLDL was increased by the presence of the site 1 ligand PIP₃ as cpd984 increased binding only to the fed fraction of VLDL, which we propose to be a condition for generation of this signaling molecule near where apo B and VLDL are synthesized and incorporated into the ER in liver cells (Figure 5A,B).

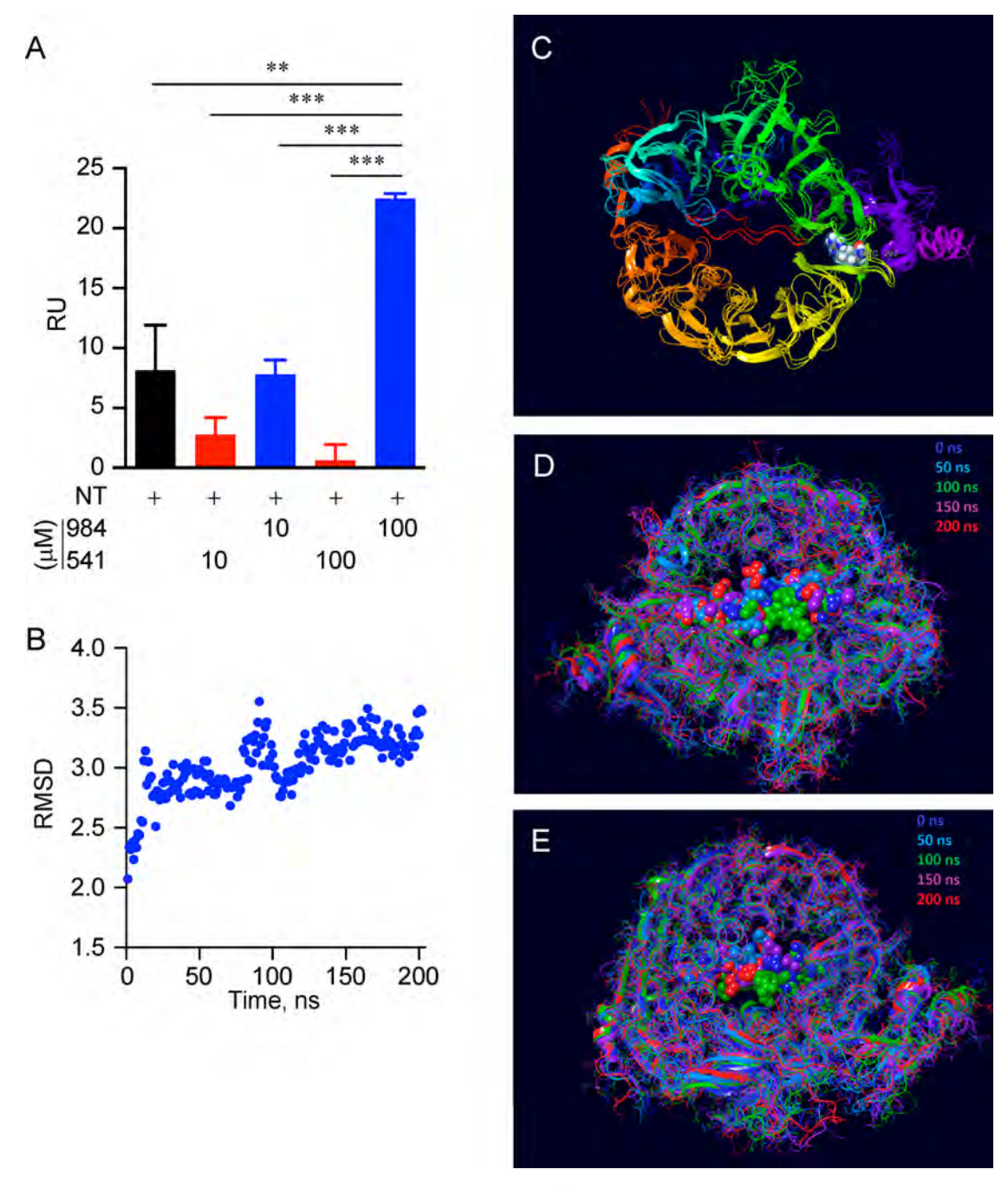


Figure 6. Dynamics of binding of full length NT to the sortilin luminal domain. (A) SPR analysis following administration of 100 nM NT alone and in the presence of either cpd984 or cpd541 at concentrations of 10 and 100 μ M. RU subtractions of cpd984 and cpd541 alone were performed for injections at the corresponding concentrations in the presence of neurotensin to depict the effect of these compounds on the binding of neurotensin to sortilin. Canonical binding to sortilin site 1 was demonstrated by competition of cpd541 for binding of NT to sortilin. Noncanonical binding of site 2 by cpd984 enhanced binding of NT to sortilin. (B) RMSD of the 200 ns MD simulation of full length NT across the central cavity of sortilin based on PDB entry 4PO7. (C) NT backbone strands taken at 0, 100, and 200 ns. (D) Space filling model of NT bound to sortilin taken from a vantage point opposite the transmembrane attachment site of the aligned slices of sortilin molecular dynamics simulations with 0 ns in gray, 50 ns in light blue, 100 ns in light green, 150 ns in purple, and 200 ns in red. (E) Space filling model of the same poses as in panel D taken from the vantage point of facing the transmembrane attachment site of sortilin. Error bars represent the SEM (n = 3). **p < 0.01, and ***p < 0.001 (one-way ANOVA with multiple comparisons).

We previously showed that circulating VLDL contains more PIP₃ than LDL. ¹⁸ We thus predicted that VLDL would bind sortilin with an affinity that was higher than that of LDL. For this purpose, we purified VLDL and LDL from rat plasma and tested sortilin binding by SPR and MST. The $K_{\rm D}$ for VLDL was between 4 and 5 nM and the $K_{\rm D}$ for LDL was between 54 and 74

nM using fits generated from GE Biacore T200 Evaluation Software version 3.2 (Figure 5E); these values were comparable with the average $K_{\rm D}$ obtained using Nanotemper M.O. Affinity Analysis Software version 2.1.5 (Figure 5D), which were plotted in GraphPad Prism version 8.4.3 using a one-site specific binding model and a sigmoidal model for SPR and MST, respectively.

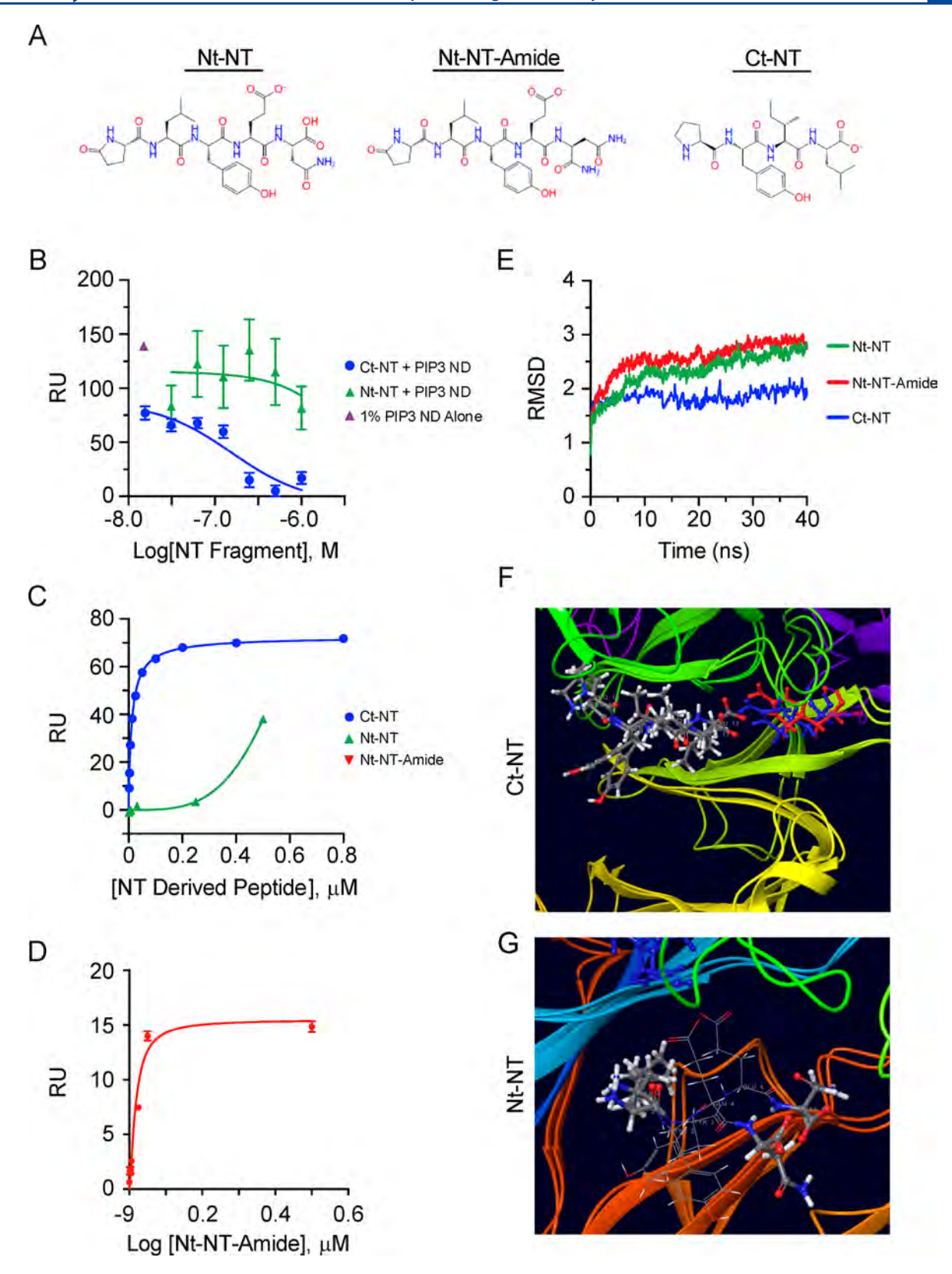


Figure 7. NT as a small molecule probe and development of a novel NT sortilin probe. (A) Structures of NT fragments. (B) Sortilin SPR using NT fragments from PDB entry 4PO7 showing Ct-NT inhibits the binding of sortilin to 79/20/1 PC/PE/PIP₃ nanodiscs whereas the Nt-NT shows no binding. (C) SPR traces of binding of Nt-NT and Ct-NT to immobilized sortilin. (D) SPR trace of binding of Nt-NT-amide to sortilin. (E) RMSD of MD of triplicate 50 ns simulations of NT fragments. (F) Representative pre- and post-MD simulation with both structures aligned and R292 for the start of the simulation shown in blue and red at the end of the simulation, respectively, indicating maintenance of the salt bridge with Ct-NT. (G) Representative pose of the Nt-NT-amide fragment bound to the hydrophobic pocket of site 2 with the amide bond facing away from the hydrophobic pocket of sortilin.

The lipoproteins were analyzed for PIP₃ content and determined to be consistent with previous results¹⁸ (Figure 5D,E). We hypothesized that this binding affinity difference was due to differences in particle composition, where VLDL acquired PIP₃ during co-synthesis with apo B. These data suggest the differences between LDL and VLDL binding were independent of apo B, as both particle types contain the protein, suggesting that the primary causative factor for the binding affinity difference to be the presence of another ligand, which we hypothesize to be PIP₃.

Cpd984 and Neurotensin Binding to Sortilin Site 1. Thus far, this study has focused on the effect of cpd984 on the binding of hepatocyte cargo to sortilin. To test if cpd984 had effects similar to those of cargo from another tissue such as neuronal tissue, we tested the effect of this compound on the characterized binder of sortilin, neurotensin or NT. Using SPR, we monitored the binding of NT to sortilin and found that cpd541 competed for binding of NT to sortilin in a dosedependent fashion (Figure 6A). In contrast, cpd984 enhanced the binding of NT to sortilin in a dose-dependent fashion.²⁷ As NT binding has been shown to be mainly guided by site 1 interactions, we hypothesize that cpd541 functions as an inhibitor by binding to site 1 to compete off binding of NT to sortilin. 47 The effects of cpd984 increasing the binding of NT to sortilin suggest that the primary interaction of NT was with site 1 of sortilin.

We previously hypothesized that NT binds across the sortilin β -propeller cavity connecting site 1 with site 2 of sortilin in line with previous observations from the structural biology groups responsible for determining the structure of sortilin at various concentrations of NT. ^{27,48} We now show the results of an MD simulation utilizing our previously predicted NT-sortilin structure. Over the course of a 200 ns simulation, full length NT stayed stably bound across the sortilin β -propeller throughout this and two other 100 ns simulations. The RMSD over the course of the 200 ns trajectory is presented (Figure 6B). To visualize the movement of NT, we took NT poses from 0, 100, and 200 ns slices of the simulation and overlaid them to show their proximity to R292, demonstrating that NT stayed stably bound to R292 over the course of the 200 ns simulation (Figure 6C). While the strands differed in their positioning across the central cavity of the β -propeller, they stayed stably bound to the hydrophobic pocket of site 2 in addition to site 1 of sortilin. Variability in the NT alignment across the β -propeller central cavity was found when five slices of the 200 ns simulation were exported at 50 ns intervals, and the strands of NT were colored according to the time of the simulation. These simulations were aligned using Schrödinger's Maestro, and results are shown for the front and back of the propeller central cavity (Figure 6D,E) bound to full length NT, indicating that both halves of NT stayed bound across the central cavity over the course of the 100 ns simulation. These results indicated that there was variability in the conformation of NT in the center of the cavity of sortilin. We propose that the additional amino acids connecting the C-terminal and N-terminal portions of NT are not required for physical binding to sortilin and therefore could have an additional role in modulating sortilin. These simulations taken together support the idea that NT stays stably bound to site 1 and that it serves as a bona fide ligand for site 1 binding as previously suggested, though it may include some cooperative binding from site 2 as we showed C-terminal NT to bind with lower affinity than full length NT and we now show stable site 2

binding of NT over the course of a medium length MD simulation. ¹⁸

Neurotensin Fragments Utilized to Define Site **Specific Sortilin Probes.** MD simulations showed that NT stably associates with both site 1 and site 2 of sortilin. To determine the dynamics of binding of both ends of NT with sortilin, we generated four-amino acid constructs of the N- and C-termini of NT (Figure 7A). First, we examined the effects of these NT truncations on the binding of PIP3 by sortilin using nanodiscs containing 1% PIP₃. This showed binding of PIP₃ to sortilin was inhibited by the C-terminal fragment of NT (Ct-NT) with an IC₅₀ of 157 nM using GraphPad Prism version 8.4.3 and a 95% confidence interval of 43-557 nM in line with our previously reported K_D for binding of Ct-NT to sortilin of 138 nM. 18 This is in contrast to essentially no inhibition upon administration of similar concentrations of the N-terminal fragment of NT (Nt-NT) (Figure 7B). This is in agreement with simulations showing that the C-terminus of NT interacts with site 1, where PIP3 binds. The lack of an effect of Nt-NT was in keeping with our previous report as well as a report from Quistgaard et al., which indicated that Nt-NT did not bind to sortilin. 18,47 While this was similar to other findings, it did not reflect the modeling showing that full length NT interacted with both site 1 and site 2 of sortilin. We theorized that the Cterminal carboxylate of Nt-NT could prevent interactions with the central portion of the β -propeller. To test this, we modified the C-terminal end (PDB entry 4PO7) to replace the terminal carboxylate with an amide, which we term Nt-NT-amide. This allowed the Nt-NT-amide to bind site 2 with a K_D of ~170 nM using a one-site specific binding model in GraphPad Prism version 8.4.3, which was close to the affinity of Ct-NT for binding site 1, with a K_D of ~120 nM using the same model (Figure 7C).

We extended our MD analysis of these NT fragments to determine if they stably bound to sortilin, and whether the Nterminal pose generated in site 2 of sortilin from PDB entry 4PO7 was biologically relevant. This showed that the Nt-NT, Nt-NT-amide, and Ct-NT fragments were stably bound to sortilin over the course of 50 ns simulations (n = 3 for each type of simulation). Interestingly, there was more overall flux in the backbone of sortilin for the two site 2 N-terminal NT simulations (n = 3 for each) on average across these six simulations as compared to the Ct-NT simulations, with a slight increase for the Nt-NT-amide fragment over the Nt-NTcarboxylate fragment (Figure 7E). Final poses from all three Cterminal (Figure 7F) and N-terminal NT (Figure 7G) simulations are shown indicating stable salt bridge formation of Arg292 with the C-terminal carboxylate of Ct-NT and burying of the N-terminal portion of NT opposite the end of the C-terminal carboxylate or amide. These data indicate the usefulness of NT fragments for analysis of site specific binding of sortilin and validate our previous observations of small molecule probe specificity for sortilin.

A Model for Allosteric Regulation of Sortilin Binding. This study has shown that engaging site 2 of sortilin results in demonstrable consequences for sorting of sortilin cargo that depend on site 1 of sortilin for secretion. We now propose a model for site specific regulation of sortilin trafficking, including a model for how the administration of site 1 and site 2 specific sortilin binding molecules results in altered hepatic protein trafficking (Figure 8). In this model, cpd984 binds to site 2 and induces conformational changes allowing greater binding of VLDL to sortilin through site 1 interactions. Increased binding

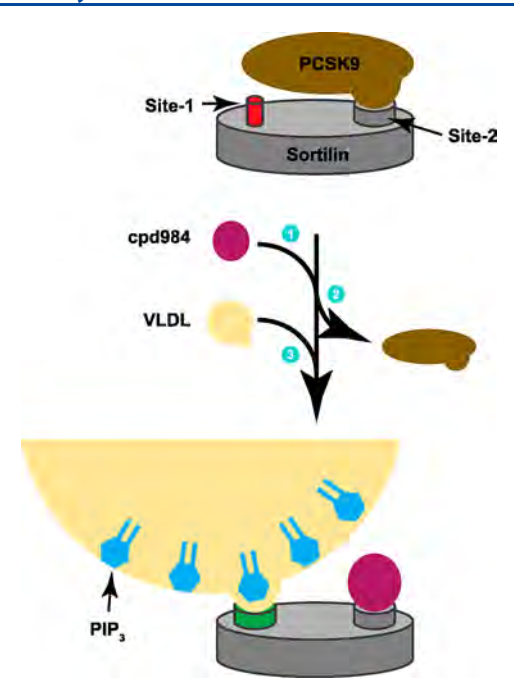


Figure 8. Model for allosteric regulation of sortilin binding. Shown is a schematic representing the allosteric effect of binding of site 2 with cpd984 and its effects on site 1 binding by VLDL (yellow). The sortilin β-propeller is shown with sites 1 and 2. Site 1 has a low affinity (red) for VLDL. Once cpd984 (purple) binds site 2, PCSK9 (brown) is released, and site 1 undergoes a conformational change (green) to enhance VLDL binding. VLDL is shown to have PIP₃ (cyan) to improve site 2 binding.

of VLDL to sortilin results in decreased binding of PCSK9 to sortilin due to crowding at the sortilin binding interface. The result of decreased binding of sortilin to PCSK9 is that PCSK9 is diverted away from secretion, resulting in increased cellular PCSK9 retention reflected by increased LDLR at the plasma membrane. Modulation of LDLR by inhibition of the binding of PCSK9 to LDLR is currently a front-line treatment for diseases such as hypercholesterolemia. We believe that the finding that LDLR can be modulated by targeting sortilin will be an important fundamental consideration in future treatments targeted toward achieving healthy circulation in patients with high cholesterol.

DISCUSSION

The endocytic pathway for the uptake of apo B-Lp by LDLR in hepatocytes has been studied extensively and forms much of the basis for current therapies controlling high LDL cholesterol in humans.⁴⁹ That said, little is known about the role of sortilin in this process or how the relative concentrations of receptors are regulated by sortilin. 50,51 With this understanding, we undertook studies to examine the role of sortilin in LDL and VLDL trafficking. Considering that PCSK9 is an additional ligand for sortilin-mediated secretion in hepatocytes, 50 we also explored its binding to sortilin. As part of this effort, we introduced a small molecule (cpd541) that inhibited binding of NT to sortilin at the canonical binding site (site 1). In addition, we show that the site 2 binding molecule cpd984 enhances NT-sortilin interactions in vitro, and that treatment of McA cells with cpd984 resulted in increased surface expression of LDLR as a reporter for reduced PCSK9 secretion. The absence of these

effects with the site 1 ligand cpd541 suggests that site 2 of sortilin regulates PCSK9 trafficking.

Our findings indicate that VLDL secretion is oppositely affected by administration of these two compounds. Administration of cpd984 led to increases in VLDL secretion in McA cells, whereas cpd541 inhibited VLDL secretion. These results indicate the potential for site specific modulation of sortilin chaperone activity being a primary determinant for sortilindependent VLDL trafficking outcomes in hepatocytes by blocking the interaction of sortilin with PCSK9, resulting in cellular accumulation of PCSK9. We hypothesize that cpd984 treatment of McA cells results in the cellular accumulation of PCSK9. This hypothesis is supported by increased cellular LDLR, which reflects inhibited PCSK9 secretion, as decreased PCSK9 secretion would prevent the internalization and degradation of LDLR. These results are consistent with what is known about the effect of PCSK9 on reducing the amount of LDLR available to remove circulating LDL from the bloodstream. However, it is not clear what effect this will truly have on circulating LDL because of the balance between secretion and degradation rates. Overall, these results suggest that site 2 is the binding site for PCSK9 trafficking in hepatic cells. We hypothesize that sortilin in the secretory pathway is ratelimiting, so when more is bound to VLDL, less is available for PCSK9 secretion.

Together, these results present a complex interconnected regulatory system for hepatic apo B lipoprotein metabolism that is rooted in the mechanisms of protein sorting by the orthologue of yeast Vps10, sortilin. Considering the complexity of this system, our observations on sortilin regulation in hepatocytes may serve to support new paradigms for sortilin trafficking in other cell types, including neuronal and adipose cells. Specifically, these studies may help in understanding insulin secretion, 11,18,27 Glut4 transport, 52–55 and plaque formation in Alzheimer's disease. 56–58

In hepatocytes, sortilin plays a central role in apo B-Lp metabolism, yet its exact role remains enigmatic. 15 Significant questions about how sortilin knockdowns both increase and decrease hepatic VLDL secretion remain, ¹³ and as do questions of whether separate VLDL ligands interact on the VLDL surface when binding to sortilin. Considering the complexity of these questions, we propose a model in which sortilin contains at least two interactive sites for ligand binding. We also suggest that an allosteric conformational change exists where binding site 2 induces tighter binding of cargo to site 1. This was exhibited by the effects of cpd984 on the binding of NT to site 1 and could also explain why full length NT binds sortilin more strongly than Ct-NT. Overall, we think that the use of site 2-directed sortilin binding molecules such as cpd984 may be useful clinically to increase LDLR expression; however, care should be taken with respect to increased VLDL secretion. It is envisioned by the authors that a site 2 molecule may be used in a cocktail with PCSK9/LDLR disruptors such as the monoclonal antibody treatment Repatha, though no experiments were conducted to examine this effect. Furthermore, approaches could be developed to selectively regulate the involved pathways by specifically targeting either site of sortilin. Such strategies could potentially reduce apo B 100 secretion to lower the risk of atherosclerosis or increase VLDL secretion in an attempt to modulate hepatic triglyceride secretion to reduce hepatic steatosis.²⁷ To help delineate sites 1 and 2 of sortilin, we developed a novel NT-based probe to site 2 of sortilin and showed that cpd984 behaves like this compound. We hope this

will help researchers further understand the complicated nature of sortilin trafficking with respect to site specific modulation of trafficking patterns dependent on the protein sortilin

An appealing hypothesis based on these observations is that VLDL particle composition directs trafficking of PCSK9 in hepatocytes. The discovery of a second ligand binding site on sortilin that regulates PCSK9 binding and cell retention when bound is novel. The allosteric effect of binding to site 2 in increasing the binding of the ligand to site 1 offers therapeutic potential in regulating VLDL secretion while enhancing VLDL remnant clearance by LDLR, which would be augmented by decreased LDLR degradation.

AUTHOR INFORMATION

Corresponding Author

Rutilio A. Fratti — Department of Biochemistry and Center for Biophysics and Quantitative Biology, University of Illinois Urbana-Champaign, Urbana, Illinois 61801, United States; orcid.org/0000-0001-9109-6666; Phone: (217) 244-5513; Email: rfratti@illinois.edu; Fax: (217) 244-5858

Authors

Robert P. Sparks — Department of Biochemistry, University of Illinois Urbana-Champaign, Urbana, Illinois 61801, United States

Andres S. Arango — Center for Biophysics and Quantitative Biology, University of Illinois Urbana-Champaign, Urbana, Illinois 61801, United States; orcid.org/0000-0003-2278-3619

Jermaine L. Jenkins — Structural Biology & Biophysics Facility, University of Rochester Medical Center, Rochester, New York 14642, United States

Wayne C. Guida — Department of Chemistry, University of South Florida, Tampa, Florida 33620, United States

Emad Tajkhorshid — Department of Biochemistry, Center for Biophysics and Quantitative Biology, and Beckman Institute for Advanced Science & Technology, University of Illinois Urbana-Champaign, Urbana, Illinois 61801, United States; orcid.org/0000-0001-8434-1010

Charles E. Sparks – Department of Pathology & Laboratory Medicine, University of Rochester Medical Center, Rochester, New York 14642, United States

[∇]Janet D. Sparks – Department of Pathology & Laboratory Medicine, University of Rochester Medical Center, Rochester, New York 14642, United States

Complete contact information is available at: https://pubs.acs.org/10.1021/acs.biochem.0c00741

Author Contributions

R.P.S. and J.D.S. contributed equally to this work. R.P.S., J.D.S., A.S.A., C.E.S., and R.A.F. conceived the project and designed experiments. R.P.S., J.D.S., A.S.A., and J.L.J. performed the experiments and analyzed data. W.C.G. and E.T. provided software and provided funding. J.D.S., C.E.S., and R.A.F. supervised the research. R.P.S., A.S.A., J.D.S., C.E.S., and R.A.F. wrote the manuscript with input from all authors.

Funding

This research was supported by grants from the National Institutes of General Medical Sciences (R01GM101132 to R.A.F. and P41GM104601, U01GM111251, and U54GM087519 to E.T.), the National Science Foundation, Molecular and Cellular Biology (MCB 1818310 to R.A.F.), and the Office of Naval Research (ONR N00014-16-1-2535 to

E.T.). Computational resources were provided by XSEDE (XSEDE MCA06N060) and Blue Waters (ACI1440026). SPR was aided by Dr. Jermaine Jenkins of the University of Rochester Structural Biology & Biophysics Facility with support from the National Center for Research Resources (1S10 RR027241), as well as the National Institute of Allergy and Infectious Diseases (P30AI078498) and the University of Rochester School of Medicine and Dentistry.

Notes

The authors declare no competing financial interest. $^{\nabla}$ Deceased.

DEDICATION

This paper is dedicated to Janet DeHoff Sparks. Following training at the University of Pennsylvania, Janet went on to become a Full Professor at the University of Rochester Medical Center in the Department of Pathology. Janet loved to get her work done early in the morning, go to Midtown Athletic Center, and then go right back to work to perform experiments. Janet continued this routine until her death in Sarasota, FL, from an unexpected heart attack. Many of the experiments in this paper were performed by Janet herself.

ABBREVIATIONS

apo B-Lp, apo B-containing lipoproteins; NT, neurotensin; MST, microscale thermophoresis; VLDL, very low-density lipoprotein; B100, apolipoprotein B; SPR, surface plasmon resonance; CPY, carboxypeptidase Y; McA, McCardle; PIP₃, phosphatidylinositol 3,4,5-trisphosphate.

REFERENCES

- (1) Heitman, J. (2015) On the Discovery of TOR As the Target of Rapamycin. *PLoS Pathog.* 11, e1005245.
- (2) Fitzgerald, I., and Glick, B. S. (2014) Secretion of a foreign protein from budding yeasts is enhanced by cotranslational translocation and by suppression of vacuolar targeting. *Microb. Cell Fact.* 13, 125.
- (3) Arlt, H., Reggiori, F., and Ungermann, C. (2015) Retromer and the dynamin Vps1 cooperate in the retrieval of transmembrane proteins from vacuoles. *J. Cell Sci.* 128, 645–655.
- (4) Nielsen, M. S., Madsen, P., Christensen, E. I., Nykjaer, A., Gliemann, J., Kasper, D., Pohlmann, R., and Petersen, C. M. (2001) The sortilin cytoplasmic tail conveys Golgi-endosome transport and binds the VHS domain of the GGA2 sorting protein. *EMBO J.* 20, 2180–2190.
- (5) Staudt, C., Puissant, E., and Boonen, M. (2017) Subcellular Trafficking of Mammalian Lysosomal Proteins: An Extended View. *Int. J. Mol. Sci.* 18, 47.
- (6) Leloup, N., Lössl, P., Meijer, D. H., Brennich, M., Heck, A. J. R., Thies-Weesie, D. M. E., and Janssen, B. J. C. (2017) Low pH-induced conformational change and dimerization of sortilin triggers endocytosed ligand release. *Nat. Commun.* 8, 1708.
- (7) Itoh, S., Mizuno, K., Aikawa, M., and Aikawa, E. (2018) Dimerization of sortilin regulates its trafficking to extracellular vesicles. *J. Biol. Chem.* 293, 4532–4544.
- (8) Nykjaer, A., and Willnow, T. E. (2012) Sortilin: a receptor to regulate neuronal viability and function. *Trends Neurosci.* 35, 261–270.
- (9) Kandror, K. V. (2018) The role of sortilin in the "Glut4 Pathway". Commun. Integr. Biol. 11, e1393592.
- (10) Goettsch, C., Kjolby, M., and Aikawa, E. (2018) Sortilin and Its Multiple Roles in Cardiovascular and Metabolic Diseases. *Arterioscler., Thromb., Vasc. Biol.* 38, 19–25.
- (11) Gao, A., Cayabyab, F. S., Chen, X., Yang, J., Wang, L., Peng, T., and Lv, Y. (2017) Implications of Sortilin in Lipid Metabolism and Lipid Disorder Diseases. *DNA Cell Biol.* 36, 1050–1061.

- (12) Musunuru, K., Strong, A., Frank-Kamenetsky, M., Lee, N. E., Ahfeldt, T., Sachs, K. V., Li, X., Li, H., Kuperwasser, N., Ruda, V. M., Pirruccello, J. P., Muchmore, B., Prokunina-Olsson, L., Hall, J. L., Schadt, E. E., Morales, C. R., Lund-Katz, S., Phillips, M. C., Wong, J., Cantley, W., Racie, T., Ejebe, K. G., Orho-Melander, M., Melander, O., Koteliansky, V., Fitzgerald, K., Krauss, R. M., Cowan, C. A., Kathiresan, S., and Rader, D. J. (2010) From noncoding variant to phenotype via SORT1 at the 1p13 cholesterol locus. *Nature* 466, 714–719.
- (13) Strong, A., Patel, K., and Rader, D. J. (2014) Sortilin and lipoprotein metabolism: making sense out of complexity. *Curr. Opin. Lipidol.* 25, 350–357.
- (14) Martínez-Oliván, J., Arias-Moreno, X., Velazquez-Campoy, A., Millet, O., and Sancho, J. (2014) LDL receptor/lipoprotein recognition: endosomal weakening of ApoB and ApoE binding to the convex face of the LRS repeat. FEBS J. 281, 1534–1546.
- (15) Sparks, C. E., Sparks, R. P., and Sparks, J. D. (2015) The enigmatic role of sortilin in lipoprotein metabolism. *Curr. Opin. Lipidol.* 26, 598–600.
- (16) Carlo, A. S. (2013) Sortilin, a novel APOE receptor implicated in Alzheimer disease. *Prion* 7, 378–382.
- (17) Carlo, A. S., Gustafsen, C., Mastrobuoni, G., Nielsen, M. S., Burgert, T., Hartl, D., Rohe, M., Nykjaer, A., Herz, J., Heeren, J., Kempa, S., Petersen, C. M., and Willnow, T. E. (2013) The pro-neurotrophin receptor sortilin is a major neuronal apolipoprotein E receptor for catabolism of amyloid-β peptide in the brain. J. Neurosci. 33, 358–370.
- (18) Sparks, R. P., Jenkins, J. L., Miner, G. E., Wang, Y., Guida, W. C., Sparks, C. E., Fratti, R. A., and Sparks, J. D. (2016) Phosphatidylinositol (3,4,5)-trisphosphate binds to sortilin and competes with neurotensin: Implications for very low density lipoprotein binding. *Biochem. Biophys. Res. Commun.* 479, 551–556.
- (19) Haas, M. E., Attie, A. D., and Biddinger, S. B. (2013) The regulation of ApoB metabolism by insulin. *Trends Endocrinol. Metab.* 24, 391–397.
- (20) Ijuin, T., and Takenawa, T. (2012) Regulation of insulin signaling by the phosphatidylinositol 3,4,5-triphosphate phosphatase SKIP through the scaffolding function of Pak1. *Mol. Cell. Biol.* 32, 3570–3584.
- (21) Kjolby, M., Nielsen, M. S., and Petersen, C. M. (2015) Sortilin, encoded by the cardiovascular risk gene SORT1, and its suggested functions in cardiovascular disease. *Curr. Atheroscler. Rep.* 17, 496.
- (22) Mazella, J., Zsürger, N., Navarro, V., Chabry, J., Kaghad, M., Caput, D., Ferrara, P., Vita, N., Gully, D., Maffrand, J. P., and Vincent, J. P. (1998) The 100-kDa neurotensin receptor is gp95/sortilin, a non-G-protein-coupled receptor. *J. Biol. Chem.* 273, 26273–26276.
- (23) Chamberlain, J. M., O'Dell, C., Sparks, C. E., and Sparks, J. D. (2013) Insulin suppression of apolipoprotein B in McArdle RH7777 cells involves increased sortilin 1 interaction and lysosomal targeting. *Biochem. Biophys. Res. Commun.* 430, 66–71.
- (24) Sparks, J. D., Magra, A. L., Chamberlain, J. M., O'Dell, C., and Sparks, C. E. (2016) Insulin dependent apolipoprotein B degradation and phosphatidylinositide 3-kinase activation with microsomal translocation are restored in McArdle RH7777 cells following serum deprivation. *Biochem. Biophys. Res. Commun.* 469, 326–331.
- (25) Denisov, I. G., Grinkova, Y. V., Lazarides, A. A., and Sligar, S. G. (2004) Directed self-assembly of monodisperse phospholipid bilayer Nanodiscs with controlled size. *J. Am. Chem. Soc.* 126, 3477–3487.
- (26) Sparks, J. D., Chamberlain, J. M., O'Dell, C., Khatun, I., Hussain, M. M., and Sparks, C. E. (2011) Acute suppression of apo B secretion by insulin occurs independently of MTP. *Biochem. Biophys. Res. Commun.* 406, 252–256.
- (27) Sparks, R. P., Guida, W. C., Sowden, M. P., Jenkins, J. L., Starr, M. L., Fratti, R. A., Sparks, C. E., and Sparks, J. D. (2016) Sortilin facilitates VLDL-B100 secretion by insulin sensitive McArdle RH7777 cells. *Biochem. Biophys. Res. Commun.* 478, 546–552.
- (28) Sparks, J. D., Phung, T. L., Bolognino, M., Cianci, J., Khurana, R., Peterson, R. G., Sowden, M. P., Corsetti, J. P., and Sparks, C. E. (1998) Lipoprotein alterations in 10- and 20-week-old Zucker diabetic fatty rats: hyperinsulinemic versus insulinopenic hyperglycemia. *Metab., Clin. Exp.* 47, 1315–1324.

- (29) Halgren, T. A., Murphy, R. B., Friesner, R. A., Beard, H. S., Frye, L. L., Pollard, W. T., and Banks, J. L. (2004) Glide: a new approach for rapid, accurate docking and scoring. 2. Enrichment factors in database screening. *J. Med. Chem.* 47, 1750–1759.
- (30) Phillips, J. C., Braun, R., Wang, W., Gumbart, J., Tajkhorshid, E., Villa, E., Chipot, C., Skeel, R. D., Kalé, L., and Schulten, K. (2005) Scalable molecular dynamics with NAMD. *J. Comput. Chem.* 26, 1781–1802.
- (31) Huang, J., Rauscher, S., Nawrocki, G., Ran, T., Feig, M., de Groot, B. L., Grubmüller, H., and MacKerell, A. D. (2017) CHARMM36m: an improved force field for folded and intrinsically disordered proteins. *Nat. Methods* 14, 71–73.
- (32) Feller, S. E., Zhang, Y., Pastor, R. W., and Brooks, B. R. (1995) Constant Pressure Molecular Dynamics Simulation: The Langevin Piston Method. *J. Chem. Phys.* 103, 4613–4621.
- (33) Martyna, G. J., Tobias, D. J., and Klein, M. L. (1994) Constant Pressure Molecular Dynamics Algorithms. *J. Chem. Phys.* 101, 4177–4189
- (34) Darden, T., York, D., and Pedersen, L. G. (1993) Particle Mesh Ewald: An N·log(N) Method for Ewald Sums in Large Systems. *J. Chem. Phys.* 98, 10089–10092.
- (35) Essmann, U., Perera, L., Berkowitz, M. L., Darden, T., Lee, H., and Pedersen, L. G. (1995) A Smooth Particle Mesh Ewald: An N-log(N) Method for Ewald Sums in Large Systems. *J. Chem. Phys.* 103, 8577–8593.
- (36) Miyamoto, S., and Kollman, P. A. (1992) SETTLE: An Analytical Version of the SHAKE and RATTLE Algorithm for Rigid Water Molecules. *J. Comput. Chem.* 13, 952–962.
- (37) Humphrey, W., Dalke, A., and Schulten, K. (1996) VMD Visual Molecular Dynamics. *J. Mol. Graphics* 14, 33–38.
- (38) Trott, O., and Olson, A.J. (2010) AutoDock Vina: improving the speed and accuracy of docking with a new scoring function, efficient optimization, and multithreading. *J. Comput. Chem.* 31, 455–461.
- (39) Beauchamp, K. A., Bowman, G. R., Lane, T. J., Maibaum, L., Haque, I. S., and Pande, V. S. (2011) MSMBuilder2: Modeling Conformational Dynamics at the Picosecond to Millisecond Scale. *J. Chem. Theory Comput.* 7, 3412–3419.
- (40) Pande, V. S., Beauchamp, K., and Bowman, G. R. (2010) Everything you wanted to know about Markov State Models but were afraid to ask. *Methods* 52, 99–105.
- (41) Gowers, R. J., Linke, M., Barnoud, J., Reddy, T. J. E., Melo, M. N., Seyler, S. L., Dotson, D. L., Domanski, J., Buchoux, S., Kenney, I. M., and Beckstein, O. (2016) MDAnalysis: A Python package for the rapid analysis of molecular dynamics simulations. *Proceedings of the 15th Python in Science Conference*, pp 98–105.
- (42) Michaud-Agrawal, N., Denning, E. J., Woolf, T. B., and Beckstein, O. (2011) MDAnalysis: a toolkit for the analysis of molecular dynamics simulations. *J. Comput. Chem.* 32, 2319–2327.
- (43) Sparks, R. P., and Fratti, R. (2019) Use of Microscale Thermophoresis (MST) to Measure Binding Affinities of Components of the Fusion Machinery. *Methods Mol. Biol.* 1860, 191–198.
- (44) Sparks, R. P., Arango, A. S., Starr, M. L., Aboff, Z. L., Hurst, L. R., Rivera-Kohr, D. A., Zhang, C., Harnden, K. A., Jenkins, J. L., Guida, W. C., Tajkhorshid, E., and Fratti, R. A. (2019) A small-molecule competitive inhibitor of phosphatidic acid binding by the AAA+protein NSF/Sec18 blocks the SNARE-priming stage of vacuole fusion. *J. Biol. Chem.* 294, 17168–17185.
- (45) Starr, M. L., Sparks, R. P., Arango, A. S., Hurst, L. R., Zhao, Z., Lihan, M., Jenkins, J. L., Tajkhorshid, E., and Fratti, R. A. (2019) Phosphatidic acid induces conformational changes in Sec18 protomers that prevent SNARE priming. *J. Biol. Chem.* 294, 3100–3116.
- (46) Bochevarov, A. D., Harder, E., Hughes, T. F., Greenwood, J. R., Braden, D. A., Philipp, D. M., Rinaldo, D., Halls, M. D., Zhang, J., and Friesner, R. A. (2013) Jaguar: A high-performance quantum chemistry software program with strengths in life and materials sciences. *Int. J. Quantum Chem.* 113, 2110–2142.
- (47) Quistgaard, E. M., Grøftehauge, M. K., Madsen, P., Pallesen, L. T., Christensen, B., Sørensen, E. S., Nissen, P., Petersen, C. M., and Thirup, S. S. (2014) Revisiting the structure of the Vps10 domain of

- human sortilin and its interaction with neurotensin. Protein Sci. 23, 1291–1300.
- (48) Trabjerg, E., Abu-Asad, N., Wan, Z., Kartberg, F., Christensen, S., and Rand, K. D. (2019) Investigating the Conformational Response of the Sortilin Receptor upon Binding Endogenous Peptide- and Protein Ligands by HDX-MS. *Structure* 27, 1103—1113.e3.
- (49) Nair, P. (2013) Brown and Goldstein: the cholesterol chronicles. *Proc. Natl. Acad. Sci. U. S. A. 110*, 14829–14832.
- (50) Gustafsen, C., Kjolby, M., Nyegaard, M., Mattheisen, M., Lundhede, J., Buttenschøn, H., Mors, O., Bentzon, J. F., Madsen, P., Nykjaer, A., and Glerup, S. (2014) The hypercholesterolemia-risk gene SORT1 facilitates PCSK9 secretion. *Cell Metab.* 19, 310–318.
- (51) Wolf, D. H., and Schäfer, A. (2005) CPY* and the power of yeast genetics in the elucidation of quality control and associated protein degradation of the endoplasmic reticulum. *Curr. Top Microbiol Immunol* 300, 41–56.
- (52) Kioumourtzoglou, D., Pryor, P. R., Gould, G. W., and Bryant, N. J. (2015) Alternative routes to the cell surface underpin insulin-regulated membrane trafficking of GLUT4. *J. Cell Sci.* 128, 2423–2429.
- (53) Morris, N. J., Ross, S. A., Lane, W. S., Moestrup, S. K., Petersen, C. M., Keller, S. R., and Lienhard, G. E. (1998) Sortilin is the major 110-kDa protein in GLUT4 vesicles from adipocytes. *J. Biol. Chem.* 273, 3582–3587.
- (54) Pan, X., Zaarur, N., Singh, M., Morin, P., and Kandror, K. V. (2017) Sortilin and retromer mediate retrograde transport of Glut4 in 3T3-L1 adipocytes. *Mol. Biol. Cell* 28, 1667–1675.
- (55) Shi, J., and Kandror, K. V. (2005) Sortilin is essential and sufficient for the formation of Glut4 storage vesicles in 3T3-L1 adipocytes. *Dev. Cell* 9, 99–108.
- (56) Capsoni, S., Carlo, A. S., Vignone, D., Amato, G., Criscuolo, C., Willnow, T. E., and Cattaneo, A. (2012) SorLA deficiency dissects amyloid pathology from tau and cholinergic neurodegeneration in a mouse model of Alzheimer's disease. *J. Alzheimer's Dis.* 33, 357–371.
- (57) Ruan, C. S., Liu, J., Yang, M., Saadipour, K., Zeng, Y. Q., Liao, H., Wang, Y. J., Bobrovskaya, L., and Zhou, X. F. (2018) Sortilin inhibits amyloid pathology by regulating non-specific degradation of APP. *Exp. Neurol.* 299, 75–85.
- (58) Zhao, Y., Cui, J. G., and Lukiw, W. J. (2007) Reduction of sortilin-1 in Alzheimer hippocampus and in cytokine-stressed human brain cells. *NeuroReport* 18, 1187–1191.